Robust and Natural Physical Adversarial Examples for Object Detectors

Mingfu Xue^a, Chengxiang Yuan^a, Can He^a, Jian Wang^a, Weiqiang Liu^b

^aCollege of Computer Science and Technology, Nanjing University of Aeronautics and Astronautics, Nanjing, China ^bCollege of Electronic and Information Engineering, Nanjing University of Aeronautics and Astronautics, Nanjing, China

Abstract

Recently, many studies show that deep neural networks (DNNs) are susceptible to adversarial examples, which are generated by adding imperceptible perturbations to the input of DNN. However, in order to convince una auversarial examples are real uncans in real physical world, it is necessary to study and evaluate the adversarial examples in real-world scenarios. In this paper, we propose a robust and natural physical adversarial example attack method targeting object detectors under real-world conditions, which is more challenging than targeting image classifiers. The generated adversarial examples are robust to various physical constraints and visually look similar to the original images, thus these adversarial examples are natural to humans and will not cause any suspicions. First, to ensure the robustness of the adversarial examples are natural to humans and will not cause any suspicions. First, to ensure the robustness of the adversarial examples are natural to humans and will not cause any suspicions. First, to ensure the robustness of the adversarial examples are natural to humans and will not cause any suspicions. First, to ensure the robustness of the adversarial examples are natural to humans and will not cause any suspicions. First, to ensure the robustness of the adversarial examples are natural to humans and will not constraints and visually look similar to the original images and evaluate that of the adversarial examples and intensities of the added perturbations, and utilizes the real-world perturbations socre (*RPS*) to make the perturbations be similar to those real noises in physical world. Compared with existing studies, our generated adversarial examples are robust under various indoor and outdoor physical conditions, including different distances, angles, illuminations, printing chromatic aberration, and photographing. Finally, the proposed physical adversarial examples are an intensities of the added perturbations and outdoor physical conditions, including different distances, angles and illuminations, printing chromatic aberration, and photographing. Finally, the proposed physical adversarial examples in real-wor adding imperceptible perturbations to the input of DNN. However, in order to convince that adversarial examples are real threats in real physical world, it is necessary to study and evaluate the adversarial examples in real-world scenarios. In this paper, we

[16]. As a result, the adversarial examples can bring serious consequences to security and safety critical systems [17], such as autonomous vehicles and face recognition systems.

In the literature, many digital adversarial example generation methods have been proposed, such as the fast gradient sign method (FGSM) [12], the basic iterative method (BIM) [13], the momentum iterative method (MIM) [18] and the Carlini-Wagner (C&W) method [14]. In addition, a few studies [19–

Email addresses: mingfu.xue@nuaa.edu.cn (Mingfu Xue), yuancx@nuaa.edu.cn (Chengxiang Yuan), hecan@nuaa.edu.cn (Can He), wangjian@nuaa.edu.cn (Jian Wang), liuweiqiang@nuaa.edu.cn (Weigiang Liu)

function is optimized based on these images to obtain adversarial examples. Jan et al. [21] use a generative adversarial networks to simulate the physical conditions. The target of the above adversarial attacks are the image classifiers. A few other works, such as [22-25], propose adversarial attacks targeting the object detectors, which are more difficult than attacking the image classifiers. The reason is that, the image classifier can only classify an image into a single class, but the object detector needs to classify multiple objects in an image and determine the position of each object. In [22], the generated adversarial examples make the object detector produce erroneous predictions. In [23], the generated adversarial examples can make the object detector produce erroneous predictions or hide themselves from the object detector. In [24, 25], the generated adversarial examples can hide themselves from the object detector. However, the perturbations generated by the previous methods are so obvious (visually unnatural), which even affect humans' understanding of the original images and the perturbations can be easily observed. For instance, in [22], the generated adversarial examples need to add very large perturbations to fool the object detector, and even people can not distinguish the objects in the image. In [23–25], the difference between generated perturbations and the background of the original image is conspicuous, thus humans can easily perceive these anomalies in the adversarial examples.

In this paper, we propose a robust and natural physical adversarial example generation method for object detectors. For robustness, we perform a series of transformations to simulate physical conditions during the optimization process of generating an adversarial example. Besides, the proposed method uses an adaptive mask to constrain the area and intensities of added perturbations, and defines a real-world perturbation score (RPS) to optimize the perturbations at each iteration, so that the generated adversarial examples look more natural. In our experiments, we print the generated adversarial examples, and use a camera to capture the printed image in physical world. We evaluate the performances of the adversarial examples at different distances, angles, illuminations and physical scenes (indoors & outdoors), and compare with the existing works in terms of the size of added perturbations and the success rate of the adversarial examples, respectively.

The contributions of this work are as follows:

- Robustness. We propose a physical adversarial examples generation method for object detectors, which is more challenging than that targeting the image classifiers. We perform various image transformations for a generated adversarial example to ensure its robustness when facing various practical conditions, including different angles, distances, illuminations, scenes, printing chromatic aberration and photographing. Real-world experimental results indicate that, the attack success rate of our generated adversarial example is close to that of the adversarial examples generated by the state-of-the-art methods.
- Naturalness. We propose two novel techniques (adaptive mask and *RPS*) to constrain and optimize the added adversarial perturbations, so as to make the generated adversarial example look more natural. The adaptive mask can limit the area and intensities of the added perturbations, while the *RPS* can make the perturbations be close to realworld noises. In this way, the generated adversarial example is more natural and looks similar to the aging version (*i.e.*, eroded by rain and sunlight) of the original image. Compared with the existing works, the proposed method can obtain a good balance between the the robustness and naturalness of a generated adversarial example. The generated adversarial example can achieve a high success rate with less conspicuous perturbations, which will not cause human's suspicions.

• Transferability. The adversarial examples generated by the proposed method are proved to be transferable, which means they can generalize well between different models. Experimental results show that the adversarial examples generated based on the Faster Regions with Convolutional Neural Networks (Faster R-CNN) Inception v2 [26] model can be successfully transferred to the Single Shot Detector (SSD) Inception v2 [27], SSD MobileNet v2 [27], SSD ResNet-50 [27], You Only Look Once (YOLO) v2 [28] and YOLO v3 [29] models. Therefore, the proposed method can be used as a general method to work in black-box scenarios.

This paper is organized as follows. Section 2 reviews current deep learning based object detectors and related adversarial example attack methods. The threat model of the adversarial attack method is described in Section 3. Section 4 elaborates the proposed adversarial example generation method. Experimental evaluations in the physical conditions are presented in Section 5. Section 6 concludes this paper.

2. Preliminary

We first overview the deep learning based object detectors, which are the targets of the adversarial attacks in this work. Then, we review related adversarial example attack methods from two aspects: digital adversarial example attacks and physical adversarial example attacks.

2.1. Object detectors

Image classification and object detection are two basic tasks for machine learning models. The image classification task focuses on the overall content of an image, which aims to classify an input image into a single class. However, the object detector recognizes all the possible objects in an image, which can determine the category and location for each object. There are two different detection strategies for the current object detectors based on deep learning: 1) two-step detection strategy, such as R-CNN [30], Fast R-CNN [31] and Faster R-CNN [26]; 2) and one-step detection strategy, such as SSD [27], YOLO [32], YOLO v2 [28] and YOLO v3 [29]. The two-step object detectors first generate region proposals that may contain objects in an image, then classify the objects in each region proposal. The one-step object detectors directly predict the class and position of each object in an image by running a single Convolutional Neural Network (CNN).

2.2. Adversarial example attack methods

Given a trained machine learning model $f(\cdot)$ and an input x, the model will output a predicted label. Ideally, the predicted output should be the true label y. The adversarial attack needs to find an input x' that is similar to the original input x, but this input x' can cause the model to produce an erroneous output [14]. Generally, adversarial attacks can be divided into untargeted attacks and targeted attacks. The untargeted attack only requires to make the model output a wrong prediction [18], *i.e.*, be different from the true label y, while the targeted attack causes the

model to produce a specific label y' ($y' \neq y$). Early adversarial example attacks [12–14, 18] focus on generating digital adversarial examples, which can achieve high success rates under the laboratory/digital settings. To convince that adversarial examples are real threats in practice, some works [19–25] have proposed and evaluated the adversarial example attacks in physical conditions. However, limited to various physical constraints (e.g. distance, angle, illumination, printing chromatic aberration and photographing), those adversarial examples generated in digital domain have failed in the real world, or only achieved a low success rate [33]. Since the principle of the untargeted attack and the targeted attack are similar, we will take the untargeted attack as an example to review related digital adversarial attack methods and physical adversarial attack methods.

Digital adversarial attacks: The digital adversarial example generation methods mainly include gradient-based methods and optimization-based methods. The gradient-based methods add perturbations to the original image, which are obtained by computing the gradient of the loss function [12]. For example, in the FGSM method, the adversarial example x' is calculated as follows [12]:

$$x' = x + \epsilon \cdot sign(\nabla_x J_f(x, y)) \tag{1}$$

where the loss function $J_f(\cdot)$ calculates the difference between the predicted label of the model and the true label y. $\nabla_x J_f(x,y)$ is the gradient of the loss function, and ϵ is a hyper-parameter. This one-step gradient-based method is fast, but it is difficult to generate adversarial examples with high success rate by adding perturbations only once. Hence, many iterative gradient-based methods are proposed to generate adversarial examples. The basic iterative method for adversarial examples generation is as follow [13]:

$$x_{0}^{'} = x, \quad x_{m+1}^{'} = x_{m}^{'} + \lambda \cdot sign(\nabla_{x} J_{f}(x_{m}^{'}, y))$$
 (2)

where m is the number of iterative optimization, and λ is a hyper-parameter.

On the other hand, the optimization-based methods formulate the adversarial examples generation as an optimization problem. For instance, the Carlini-Wagner attack method [14] generates adversarial examples by minimizing the following object function [14]:

$$\arg\min_{\delta} \alpha ||\delta||_p - J_f(x + \delta, y)$$
 (3)

where $\|\delta\|_p$ is the l_p norm of the added perturbations δ , and α is a parameter used to adjust the weight of perturbations.

Physical adversarial attacks: The physical adversarial attack aims to fool the target model (image classifiers or object detectors) that deployed in the real physical world. The adversarial attacks on image classifiers only require to make the model misclassify an image. However, the adversarial attacks on object detectors need to cause the target model misclassify the objects in each detected bounding box, which are more difficult than the adversarial attacks on image classifiers. In [19–21], the authors generate physical adversarial examples for image classifiers, while in [22–25], the authors generate physical adversarial examples for object detectors.

Taking the method in [20] and [25] as examples, we describe the adversarial examples generation methods for image classifiers and for object detectors in the physical conditions, respectively. In [20], the optimization method is used to search for the perturbations δ that can fool the image classifier. To ensure the physical robustness of the generated adversarial examples, the method uses real-world images to optimize the added perturbations in the process of generating adversarial examples. The method generates adversarial examples by solving the following objective function [20]:

$$\underset{\delta}{\arg\min} \alpha ||\delta||_{p} - \frac{1}{k} \sum_{i=1}^{k} J_{f}(x_{i} + \delta, y)$$
 (4)

where x_i is an original image, and k is the number of the original images.

Zhao et al. [25] proposes two types of physical adversarial example attacks, hiding attack (HA) and appearing attack (AA). The hiding attack aims to cause the detector fail to recognize the target objects [25], while appearing attack aims to cause the detector incorrectly recognize the generated adversarial examples as the specific objects. For hiding attack [25], the authors propose the feature-interference reinforcement (FIR) [25] to enhance the robustness of adversarial examples against each hidden layer of a target DNN model. Besides, they exploit the enhanced realistic constraints generation (ERG) [25] method to perform various realistic transformations on their generated adversarial examples. For appearing attack [25], they design a nested adversarial example generation approach, which combines two different adversarial examples (AEs) into a single one. One adversarial example aims to implement the long distance attack against the object detector, and the other one is to launch the short distance attack [25].

Recently, Huang et al. [34] develop an Universal Physical Camouflage (UPC) attack for object detectors, which can attack all instances of the same target class (e.g., all cars in an input image) with the generated universal pattern. The above attack methods [22–25, 34] add the perturbations into the target objects to generate the adversarial examples, while some other works [35-37] can launch the physical adversarial attacks without manipulating the target objects. Huang et al. [35] craft an adversarial example that looks like the advertising signboard. By placing the adversarial signboard below the target objects with a certain distance, the Faster R-CNN detector fails to detect the target objects (e.g., the stop signs). Lee et al. [36] generate a physical adversarial patch, which can prevent the YOLO v3 from detecting any objects in a submitted image. Li et al. [37] directly manipulate the camera device and constructs a translucent adversarial sticker. They paste the sticker on the lens of a camera and successfully attack the DNN based classi-

However, these existing studies [25, 34] add obvious perturbations on the target objects, which cause their generated adversarial examples to be easily perceived by humans. Although the recent works [35–37] do not manipulate the target objects, their generated adversarial signboard [35] and patch [36] are very large, which make them look strange compared

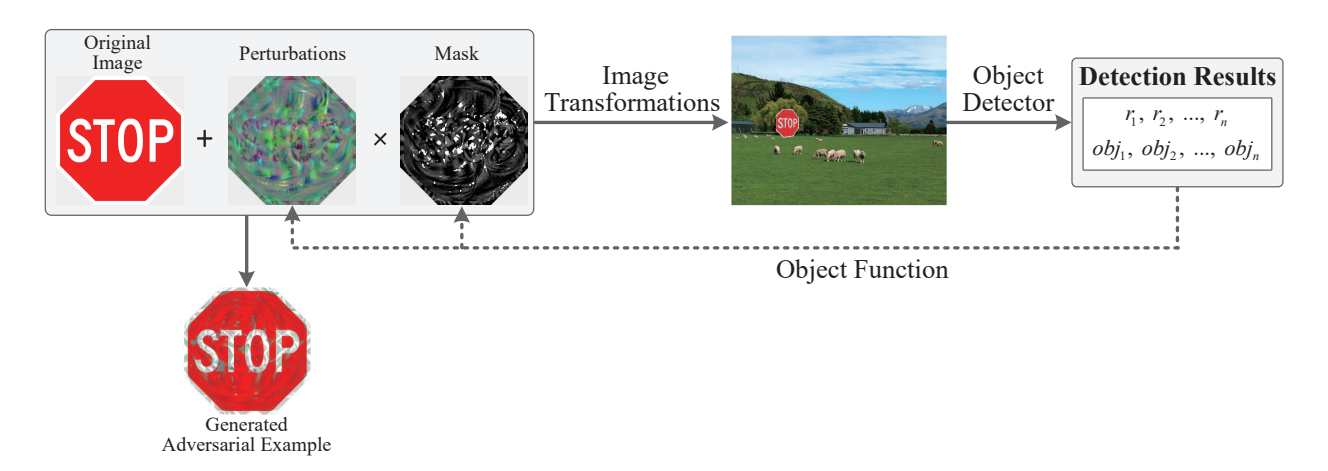


Figure 1: Overall flow of the proposed adversarial examples generation method.

to the surrounding environments. In addition, the adversarial sticker attack [37] against the camera is difficult to be conducted in real-world conditions, as the sticker can be easily observed by humans when it is pasted on the lens of the camera. Compared with these existing methods, the proposed method aims to achieve a good balance between the robustness and the naturalness of a generated adversarial example. First, we perform a series of image transformations to simulate different physical constraints during the iterative optimization, so as to ensure the robustness of our generated adversarial examples. Second, we propose two novel techniques, the adaptive mask and realworld perturbation score, to constrain the size (i.e., area and intensities) of the added perturbations and make the perturbations look like real-world noises, respectively. As a result, our generated adversarial examples can achieve robust attack performance with more natural perturbations.

3. Threat model

In this section, we describe the potential adversarial attackers in terms of the adversary's goals and adversary's abilities. Specifically, to ensure the generated adversarial examples more robust and visually more natural, we make some additional constraints on the added perturbations.

3.1. Adversary's goals

This work aims to launch the physical adversarial example attacks against the object detectors. The goal of an physical adversarial example attacker is to fool the target object detector to make incorrect predictions. Compared with the attacks on image classifiers, it is more challenging to generate adversarial examples to attack the object detectors. In this paper, we select the state-of-the-art object detector, Faster R-CNN [26], as the target of our proposed adversarial attacks. The Faster R-CNN can detect the objects in an image with a high detection accuracy and a fast detection speed [26]. Formally, given an input x, an Faster R-CNN model $f(\cdot)$, and a true label y, the object detected by Faster R-CNN on the bounding box r_i ($r_i \in rpn(x)$) is $f(x_{r_i}) = y$. The $rpn(x) = \{r_1, r_2, ..., r_n\}$ represents the collection

of bounding boxes detected by the model, where r_i is the *i*-th bounding box and n is the number of all the bounding boxes. The goal of the adversary is to add perturbations δ that satisfies the following rule to the original image:

$$f(x_{r_i} + \delta) \neq y \tag{5}$$

To ensure that the generated adversarial examples are more natural and more robust in real-world conditions, we set the following restrictions on the added perturbations:

- The added perturbations should not affect humans' understanding of the object in the original image.
- The added perturbations should not be too anomalous and should be similar to real-world noises. In this way, the generated adversarial examples are more natural and will not arouse human's suspicions.
- The added perturbations should be robust in various physical conditions (*e.g.*, different distances, angles, illuminations, printing chromatic aberration, photographing). In other words, the generated adversarial examples can fool the object detectors in different physical conditions.

3.2. Adversary's abilities

Generally, according to the adversary's abilities, adversarial attacks can be categorized into white-box attacks, black-box attacks and gray-box attacks. In this work, adversaries generate adversarial examples in a white-box scenario. It means that adversaries have the knowledge of the target model, which includes model architectures, parameters, and weights. Although the proposed method generates adversarial examples on a white-box model, experimental results show that the adversarial examples generated by the proposed method can generalize well to other black-box models successfully. Therefore, by utilizing the transferability of the generated adversarial examples, adversaries can also carry out black-box attacks.

In real physical world, the inputs of a DNN based object detector is collected by its external camera, and an attacker cannot

directly submit the generated adversarial examples to its internal DNN model. Therefore, in this paper, we assume an adversary can only print the generated adversarial examples, and the image that captured by a camera will be used as the input of the Faster R-CNN detector.

4. The proposed attack method

4.1. Overall procedure

Fig. 1 illustrates the overall flow of the proposed adversarial examples generation method. The proposed method is based on an optimization strategy, which works as follows. First, constrained perturbations are added to the original image to generate adversarial examples. Second, image transformations are applied to the generated adversarial examples, and the transformed image is used as the input of the object detector. Third, the perturbations and the mask are further optimized by calculating the gradient of the objective function. The above iterative optimization steps are repeated until the value of the objective function is less than a predefined threshold. Finally, natural and robust physical adversarial examples are generated. Different image transformation functions are introduced in Section 4.2. The methods of constraining the added perturbations are introduced in Section 4.3.

4.2. Image transformations for simulating different physical conditions

To ensure the robustness of the generated adversarial examples in the real world, a series of image transformations are applied to these modified images. In this paper, inspired by the existing work [19], we adopt the *Expectation over Transformation (EOT)* technique [19] to perform these transformations. Such image transformations simulate the images in different physical conditions, including distance, position, angle, illumination, printing chromatic aberration, and photographing. The EOT [19] performs these transformations at each iteration of the optimization process, so as to make the added perturbations more robust. The transformation function is denoted as $t(\cdot)$, which includes the following five different transformation methods.

- **Distance transformation**: The distance transformation function first randomly adjusts the size of the image. Then, according to the size of the image, different size of Gaussian kernels are used to transform the image. The smaller the image, the larger the convolution kernel and the more blurred the transformed image is. In this way, the distance transformation function can simulate the images captured by the camera at different distances.
- Angle transformation: Angle transformation converts an image from the perspective plane to the frontal plane. By using different perspective planes, perspective transformation function can simulate the image captured by a camera at different angles.

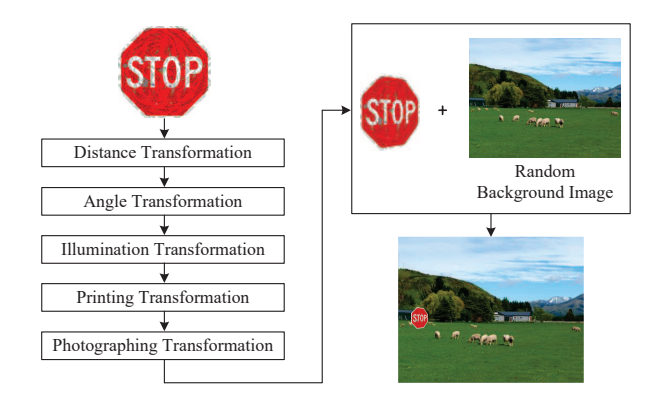


Figure 2: Process of image transformations.

- Illumination transformation: The illumination transformation function randomly adjusts the brightness and contrast of the image to simulate the image captured by a camera at different illumination conditions.
- Printing transformation: In the real world, the image captured by a camera is a printed image. Due to the chromatic aberration between the generated digital image and the printed image, the printed image may fail to fool the object detector. Therefore, in this paper, we simulate the impact of printing in the generation process with the following three steps. First, the digital image is represented by using the CMYK (cyan, magenta, yellow, black) color model [38], which has been widely used in color printing. Then, the printing transformation function adjusts the color of the image so that the chromatic aberration between the printed image and the digital image is as small as possible. Finally, the printing transformation function transfers the image from CMYK color model to RGB (red, green, blue) color model.
- **Photographing transformation**: Since the input of the object detector is the image captured by a camera, the photographing transformation function adds gaussian noises to the digital image to simulate the image captured by a camera.

The process of image transformations is shown in Fig. 2. In the optimization of each iteration, first, the generated perturbations are added to the original image, and then the above five transformation functions are applied to the image, namely $t(x + \delta)$. To ensure that the generated adversarial examples are not affected by the background, the transformed image is added to a random background image x_{bg} , namely $t(x+\delta) + x_{bg}$. For each iteration, the proposed method selects different images from the Microsoft Common Objects in Context (MS-COCO) dataset [39] as the background image. Finally, the random background containing the adversarial example is used as the input of Faster R-CNN for iterative optimization. Note that, these image transformations and background images are only used to optimize the generated adversarial example in the generation process, and the final generated physical adversarial example is the original image (e.g. a stop sign) with optimized

perturbations, which does not contain the background image and these image transformations, as shown in Fig. 1.

After obtaining the output of the object detector, the proposed method maximizes the difference between the prediction of each object and the true label. The difference is calculated as follows [23]:

$$L_f(x+\delta,y) = \mathbb{E}_{t\sim T} \left[\frac{1}{n} \sum_{r_i \in rpn(x+\delta)} J_f(t(x_{r_i}+\delta) + x_{bg}, y) \right]$$
 (6)

where $t(\cdot)$ is a transformation function, and T is the distribution of the transformation function t. Finally, the goal of the iterative optimization is to minimize the following object function:

$$\underset{\delta}{\arg\min} \alpha ||\delta||_{p} - L_{f}(x + \delta, y) \tag{7}$$

4.3. Constraining the added perturbations in adversarial examples

The perturbations generated by existing methods can fool object detectors, but these perturbations are unnatural and conspicuous. Humans can easily perceive the anomalies in the generated adversarial examples. In order to generate adversarial examples that are as similar as possible to the original image, we propose the following two methods to constrain the added perturbations. The first method uses a mask to constrain the area and intensity of the added perturbations. The second method uses real-world noises to make the added perturbations be more natural. These two methods are introduced in Section 4.3.1 and Section 4.3.2, respectively.

4.3.1. Constraining the area and intensity of perturbations with an adaptive mask

The smaller the area of perturbations added to the original image, the more natural the generated adversarial examples are. To generate adversarial examples that are as similar as possible to the original image, the proposed method uses a mask to constrain the area where perturbations are added. The mask is represented as a matrix M whose dimensions are the same as the shape of the image. The value of each pixel in the mask M ranges from 0 to 1, which indicates the intensity of the added perturbation. According to the values of these pixels in the mask, the perturbation is added to the original image by the following formulation:

$$I_{i,j} + \delta_{i,j} \cdot M_{i,j} = A_{i,j} \tag{8}$$

where $I_{i,j}$, $\delta_{i,j}$, $M_{i,j}$, and $A_{i,j}$ are the values of the ith row and the jth column on the original image (I), perturbations (δ) , mask (M), and the adversarial image (A), respectively. If the pixel value in the mask is 0, no perturbation is added to the corresponding position of the original image. If the pixel value in the mask is 1, the perturbation is added to the corresponding position of the original image directly. If the pixel value in the mask is between 0 and 1, the perturbation multiplied by this pixel value is added to the corresponding position of the original image.

The area of the added perturbations can be represented as $||M||_p$. If the value of $||M||_p$ is larger, the area of the added perturbations is larger. Otherwise, the area of the added perturbations is smaller. Since the goal of the proposed method is to make the area of the added perturbations as small as possible, the objective function can be further modified as follows:

$$\underset{\delta M}{\arg \min} \alpha ||M \cdot \delta||_p + \beta ||M||_p - L_f(x + M \cdot \delta, y)$$
 (9)

where β is a hyper-parameter for adjusting the weight of $||M||_p$. Compared with the fixed mask that used in existing works [24, 25], our proposed adaptive mask can constrain the area and intensities of generated adversarial perturbations. For an fixed mask, it will not be optimized during the whole process of the adversarial example generation, i.e., each pixel value in it remains unchanged [24, 25]. As a result, according to the Eq. 8, the intensities of these added perturbations on a target object (such as stop sign) cannot be constrained. However, for an adaptive mask, its pixel values are dynamically changed with these generated perturbations at each iterative optimization. In other words, when generating an adversarial example, we optimize the adversarial perturbations and the mask at the same time (as shown in objective function Eq. 9). Therefore, the generated perturbations on our adversarial examples are inconspicuous and can hardly been noticed.

4.3.2. Generating natural perturbations with real-world noises

In the real world, there are many real-world images that contain noises. For instance, Fig. 3 shows three examples of stop sign in the MS-COCO dataset [39]. It is shown that these real stop signs contain some real-world noises, such as graffiti and stickers. Since humans have no trouble in understanding these images with real-world noises, we aim at generating perturbations that are as similar as possible to the real-world noises. In this way, the generated adversarial examples are natural and similar to the real-world images so as not to arouse humans' suspicions.







Figure 3: Three examples of stop sign in MS-COCO dataset [39].

We select real-world images from the MS-COCO dataset [39] to extract real-world noises. These extracted real-world noises are denoted as a real-world noise set P_{real} . When generating adversarial examples, the proposed method selects the perturbations which are most similar to the noises in the real-world noise set P_{real} . Therefore, we define a metric named real-world perturbation score (RPS) to represent the similarity between the generated perturbation and the real-world noise,

which is calculated by:

$$RPS(\delta) = \sum_{p' \in \delta} \min_{p \in P_{real}} \left\| p' - p \right\|_2$$
 (10)

where δ is the perturbation vector. p' represents the pixel value in the perturbation vector δ , and p represents the pixel value of the point in the extracted real-world noise set P_{real} . If the generated perturbation is similar to the real-world noise, the value of the RPS is small. Otherwise, the value of the RPS is large. Thus, the optimization also needs to minimize the value of the RPS. Finally, after using real-world noises to constrain perturbations, the objective function of the proposed method is as follows:

$$\underset{\delta M}{\arg \min} \alpha ||M \cdot \delta||_{p} + \beta ||M||_{p} + \gamma RPS(M \cdot \delta) - L_{f}(x + M \cdot \delta, y)$$
 (11)

where γ is a hyper-parameter that controls the weight of *RPS* in the optimization process.

Note that, compared with the non-printability score (*NPS*) [40] which only focuses on the printability of generated perturbations, our proposed *RPS* considers both the printability and the visual naturalness of added perturbations. As a result, the adversarial examples generated with the *RPS* are more natural, and will not arouse humans' suspicious.

5. Experimental results

In this section, we evaluate the success rate of the generated adversarial examples on fooling object detectors in the physical conditions. First, the experimental setup is presented in Section 5.1. Then, the experimental results of physical attacks are presented in Section 5.2. Third, in Section 5.3, the adversarial examples generated by the proposed method is compared with that generated by other methods. Finally, the transferability of the adversarial examples generated by the proposed method is evaluated in Section 5.4.

5.1. Experimental setup

We use the Faster R-CNN model with Inception v2 [41] as the target model of the adversarial attack. The pre-trained model is available from [42]. In our experiment, the clean stop sign is used as the initial image, and its adversarial examples are generated with the proposed method that discussed in Section 4. We use the Konica Minolta C368 printer to print the generated adversarial examples of stop sign on A4 size paper. Then, the Nikon D3000 camera with an AF-S 18-55mm lens is used to capture the printed adversarial examples. Finally, the captured image is used as the input of Faster R-CNN to evaluate the success rate of the generated adversarial examples.

Initialization of adaptive mask M and added perturbation δ . The initialization of the adaptive mask and the added perturbations are as follows. 1) Adaptive mask. In this paper, we use an image with the shape of octagon (the same shape as the stop sign) to initialize the mask M. The position on the mask corresponds to the position on a stop sign image. Specifically, for those positions of four letters (i.e., "S", "T", "O", "P")

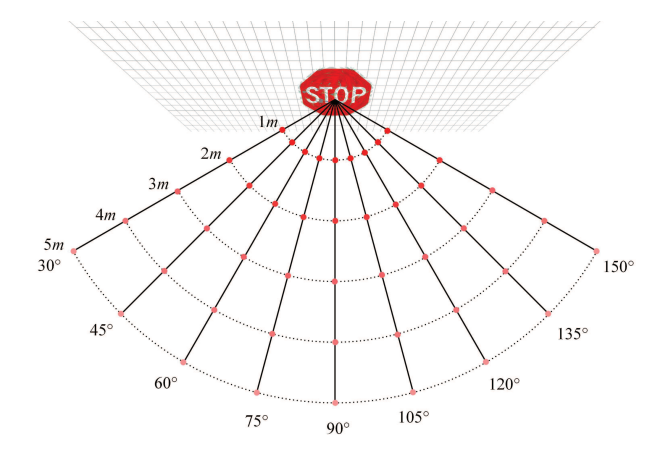


Figure 4: Different settings of the photographic distances and angles between the camera and the printed image.

and eight edge regions, the pixel values on the mask are set to be 0. The pixel values of the remaining positions (*i.e.*, the red background region) on the mask are all set to be 1. **2) Added perturbation.** The added perturbation δ is initialized by a pure white color image, *i.e.*, the *RGB* value of each pixel on the perturbation δ is set to be (255, 255, 255). These pixel values will be used as the initial perturbations to calculate the real-world perturbation score (*RPS*) and the gradient of the loss function L_f , respectively. In our experiments, the adaptive mask M and added perturbation δ are iteratively optimized by the proposed method with the objective function (Eq. 11).

To illustrate the robustness of the generated adversarial examples, we evaluate the success rate of the adversarial examples indoors and outdoors, respectively. We capture the printed image at different angles and different distances under indoor and outdoor conditions, and submit them to Faster R-CNN detector to detect. The detailed photographic distance and angle settings are shown in Fig. 4. The angle of view between the camera and the stop sign is from 30° to 150°, and the distance between the camera and the stop sign is from 1 meter to 5 meters.

Evaluation metrics. We evaluate the generated adversarial examples from the following two aspects: the success rate of adversarial examples and the naturalness of adversarial examples. First, similar to the existing works [20] and [34], we calculate the success rate R_s of adversarial examples as follows [20, 34]:

$$R_{s} = \frac{\sum_{x \in X, x' \in X'} \{ f(x_{d,a,i,s}) = y \land f(x'_{d,a,i,s}) \neq y \}}{\sum_{x \in X} \{ f(x_{d,a,i,s}) = y \}}$$
(12)

where $x_{d,a,i,s}$ represents the original image pasted on the physical scene s captured by the camera at distance d, angle a, and illumination i. Similarly, $x'_{d,a,i,s}$ represents the adversarial example pasted on the physical scene s captured by the camera at distance d, angle a, and illumination i.

Second, we use the size of the added perturbations to evaluate the naturalness of an adversarial example. If the size of added perturbations is small, the total modifications on the pixel values of an original image (*e.g.*, the stop sign) will be small as

well. As a result, the generated adversarial example is visually similar to the original image and looks natural for humans. Otherwise, the generated adversarial examples are more conspicuous. In our experiment, we use the standard Euclidean norm (L_2 -norm) to evaluate the size of the added perturbations, which is calculated as follows [43]:

$$\delta = ||X_{adv} - X_{ori}||_2 \tag{13}$$

where X_{adv} is the generated adversarial stop sign and X_{ori} is the original stop sign.

5.2. Experimental results of physical adversarial attacks

First, we evaluate the effectiveness of generated adversarial example in real physical world. Table 1 and Table 2 show the detection results of Faster R-CNN on the adversarial stop signs indoors and outdoors, respectively. These adversarial examples are captured at different photographic distances and angles. The value in parentheses represents the confidence score of Faster R-CNN in detecting the object. If an adversarial example is simultaneously detected as multiple different objects, the object with the maximum confidence level is selected as the detection result. In the experiment, the confidence threshold of Faster R-CNN is set to be 20%. If the confidence score is less than 20%, Faster R-CNN is considered to be unable to detect the target object. If the detection result of Faster R-CNN is not a stop sign or undetected, the adversarial attack is considered to be successful.

We captured the adversarial stop sign in 45 different locations indoors (in the garage), and 15 of them can successfully fool Faster R-CNN. The success rate is not high because the light in the garage is very dark and the camera can't capture such small perturbations in dark light. These generated adversarial stop signs are detected by Faster R-CNN as sport ball, vase, kite, or undetected. For example, at the distance of 1*m*, adversarial stop sign captured at 30° and 75° can successfully hide itself from the Faster R-CNN (undetected). We also captured the adversarial stop sign in 45 different locations outdoors, and 25 of them can successfully fool Faster R-CNN. These generated adversarial stop signs are detected by Faster R-CNN as cake, vase, and donut. Moreover, adversarial stop signs captured at 10 locations can hide themselves from the Faster R-CNN (undetected).

Fig. 5 illustrates some examples of successful adversarial attacks indoors and outdoors. The contents in parentheses indicate the distance, angle, indoor/outdoor illumination, and the

detection result of Faster R-CNN. It is shown that, the adversarial examples in the first three columns can make the object detector predict incorrectly, and the adversarial examples in the fourth column can hide themselves from the Faster R-CNN. The experimental results show that, the printed adversarial stop sign that captured at various angles and distances in different illuminations can successfully fool the Faster R-CNN detector, which means the generated adversarial example is effective under different physical attack scenarios. Comparing the indoor detection results with the outdoor detection results, the success rate of adversarial examples indoors is lower than that outdoors. The main reason is that, the illumination has great influences on the success rate of the generated adversarial example. The camera cannot capture such small perturbations in the adversarial stop sign in dark light conditions.

5.3. Comparison with other methods

Then, to further illustrate the naturalness and robustness of the generated adversarial examples, we compare the adversarial stop sign generated by the proposed method with that generated by [22] and [23], from the following aspects: the size of the added perturbations, the success rate of the adversarial examples indoors and outdoors.

In our experiments, we use the same printer to print the adversarial stop signs generated by [22] and [23] on A4 size papers, and use the same camera to capture photos under the same experimental conditions. Table 3 shows the comparison results of the adversarial examples generated by the proposed method with that generated by [22] and [23]. [22]-1 and [22]-2 are generated by the same method proposed in [22], but [22]-2 adds more perturbations than [22]-1. Similarly, [23]-1 and [23]-2 are adversarial stop signs generated by the same method proposed in [23], and the difference is that [23]-2 adds more perturbations than [23]-1.

Size of perturbations. The perturbations in the adversarial stop sign generated by the proposed method are much smaller than the perturbations in the adversarial stop signs generated by [22] and [23]. The size of the added perturbations generated by [22]-1, [22]-2, [23]-1, and [23]-2 are 65800.86, 95381.14, 53989.45, and 65735.61, respectively, while the size of the added perturbations generated by the proposed method is only 34969.81. In addition, as shown in Table 3, the difference between the perturbations generated by the proposed method

Table 1: Indoor detection results of Faster R-CNN or	the generated adversar	rial stop signs under diff	ferent photographic distances	and photographic angles.

Distance	30°	45°	60°	75°	90°	105°	120°	135°	150°
1 <i>m</i>	Undetected	Vase (42%)	Vase (24%)	Undetected	Stop Sign (58%)	Vase (21%)	Vase (22%)	Stop Sign (31%)	Stop Sign (95%)
2 <i>m</i>	Stop Sign (99%)	Stop Sign (99%)	Stop Sign (83%)	Stop Sign (83%)	Sport Ball (20%)	Stop Sign (58%)	Stop Sign (99%)	Stop Sign (99%)	Stop Sign (99%)
3 <i>m</i>	Stop Sign (93%)	Stop Sign (98%)	Stop Sign (98%)	Stop Sign (98%)	Stop Sign (98%)	Stop Sign (99%)	Stop Sign (92%)	Stop Sign (97%)	Stop Sign (66%)
4 <i>m</i>	Stop Sign (54%)	Stop Sign (56%)	Stop Sign (90%)	Stop Sign (94%)	Stop Sign (94%)	Stop Sign (91%)	Stop Sign (78%)	Kite (72%)	Stop Sign (46%)
5 <i>m</i>	Kite (89%)	Kite (32%)	Kite (56%)	Stop Sign (58%)	Stop Sign (59%)	Kite (70%)	Kite (91%)	Kite (62%)	Kite (83%)

Table 2: Outdoor detection results of Faster R-CNN on the generated adversarial stop signs under different photographic distances and photographic angles.

Distance	30°	45°	60°	75°	90°	105°	120°	135°	150°
1 <i>m</i>	Stop Sign (94%)	Stop Sign (98%)	Stop Sign (90%)	Stop Sign (88%)	Stop Sign (81%)	Stop Sign (67%)	Stop Sign (68%)	Stop Sign (93%)	Stop Sign (94%)
2 <i>m</i>	Vase (63%)	Undetected	Undetected	Cake (43%)	Cake (32%)	Cake (23%)	Cake (27%)	Undetected	Undetected
3 <i>m</i>	Vase (64%)	Vase (74%)	Undetected	Undetected	Donut (21%)	Undetected	Undetected	Undetected	Vase (52%)
4 <i>m</i>	Stop Sign (83%)	Stop Sign (24%)	Vase (54%)	Vase (25%)	Vase (36%)	Vase (43%)	Vase (32%)	Vase (32%)	Stop Sign (93%)
5 <i>m</i>	Stop Sign (87%)	Stop Sign (85%)	Stop Sign (88%)	Undetected	Stop Sign (86%)	Stop Sign (64%)	Stop Sign (91%)	Stop Sign (88%)	Stop Sign (91%)

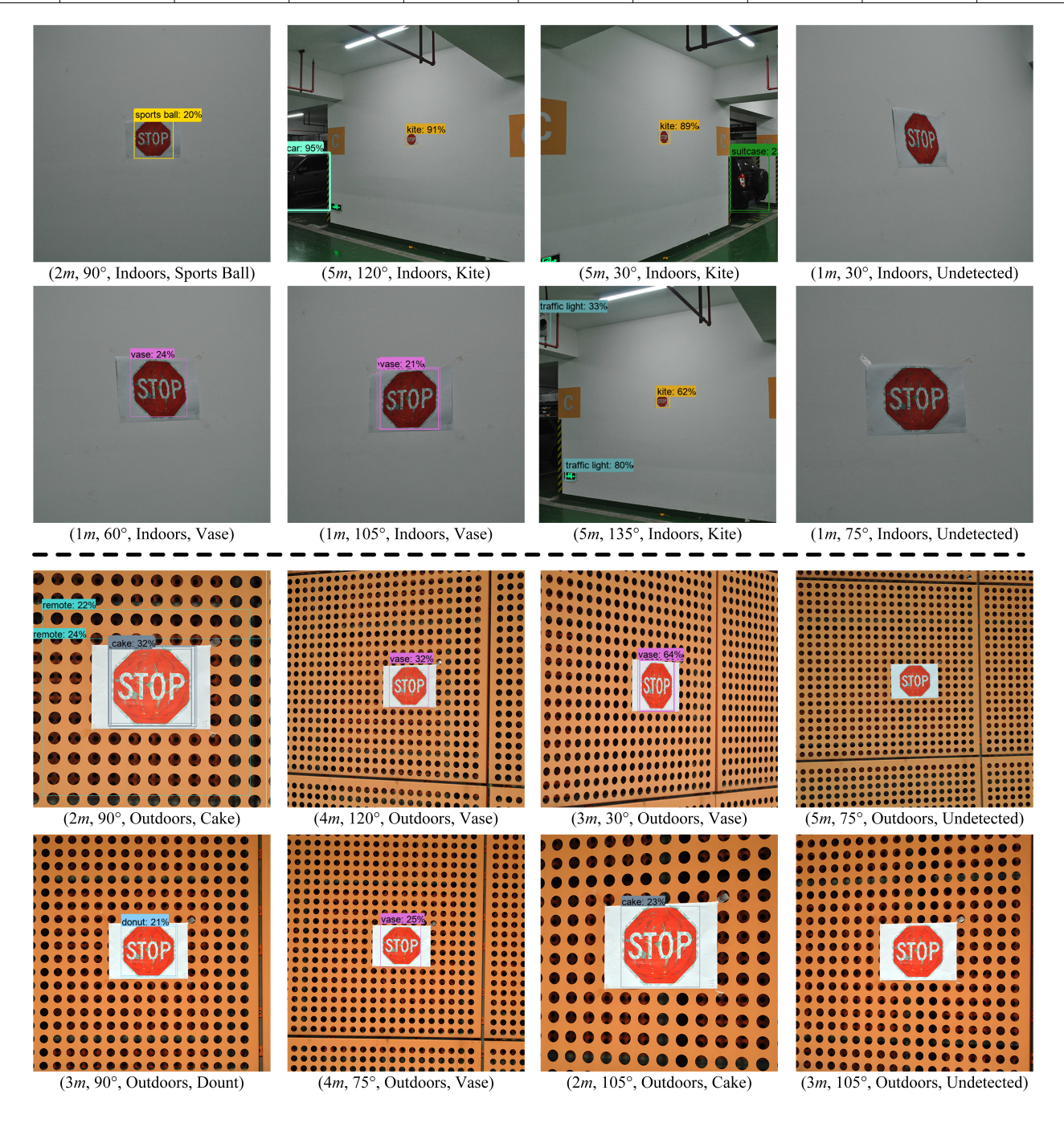


Figure 5: Examples of successful adversarial attacks. The contents in parentheses indicate the distance, angle, indoors/outdoors, and the detection result of the Faster R-CNN.

Table 3: Comparison of the proposed method and the state-of-the-art attack methods

Method	Adversarial Stop Sign Generated by the Proposed Method	Adversarial Stop Sign Generated by [22]-1	Adversarial Stop Sign Generated by [22]-2	Adversarial Stop Sign Generated by [23]-1	Adversarial Stop Sign Generated by [23]-2
Generated Adversarial Stop Sign	STOP	STOP	STOP	STOP	STOP
Size of Perturbations	34969.81	65800.86	95381.14	53989.45	65735.61
Success Rate (Indoors)	33.33%	24.44%	44.44%	37.78%	73.33%
Success Rate (Outdoors)	55.56%	15.56%	24.44%	55.56%	96.67%

and the original image is smaller than the difference between the perturbations generated by [22], [23] and the original image, which means that the added perturbations of the proposed method are more inconspicuous, and our generated adversarial stop sign looks more natural.

Attack success rate indoors and outdoors. Compared with the adversarial stop signs generated by [22], the success rate of the adversarial stop sign generated by the proposed method is higher than the success rate of [22]-1 and [22]-2 under outdoor conditions. Compared with the adversarial stop signs generated by [23], the success rate of our generated stop sign is close to the success rate of [23]-1. The success rate of the adversarial stop sign generated by the proposed method is lower than the success rate of [23]-2. The reason is that, the perturbations in [23]-2 are much larger than the perturbations in the adversarial stop sign generated by the proposed method, which makes the object detector more easier to recognize the added perturbations. However, the adversarial stop signs generated by [23]-2 is unnatural and can arouse humans' suspicions, while our generated adversarial example is more natural and looks like the aging version of a real-world stop sign. In conclusion, the adversarial examples generated by the proposed method can achieve a high attack success rate with less conspicuous perturbations.

5.4. Transferability across different target models

Finally, to evaluate the proposed method in black-box scenarios, we also evaluate the transferability of the generated adversarial examples on different object detectors. Firstly, we generate adversarial examples based on a white-box model. Then, these generated adversarial examples are evaluated on other black-box models. In this experiment, the Faster R-CNN [26] Inception v2 model is used as the white-box model, and the Faster R-CNN ResNet-50 [26], Faster R-CNN ResNet-101 [26], SSD Inception v2 [27], SSD MobileNet v2 [27], SSD ResNet-50 [27], YOLO v2 [28], and YOLO v3 [29] models are used as black-box models. We download the pre-trained Faster R-CNN and SSD object detectors from [42], and the two pre-trained YOLO object detectors are available in [44]. The

detection structures of Faster R-CNN Inception v2, Faster R-CNN ResNet-50, and Faster R-CNN ResNet-101 are similar. The difference between them is that they use different feature extractors to process the image before detecting the object. The detection structures of SSD Inception v2, SSD MobileNet v2, SSD ResNet-50, YOLO v2, and YOLO v3 are different from the detection structure of Faster R-CNN Inception v2.

Table 4 shows the success rate of the generated adversarial examples on the white-box model and black-box models. First, it is shown that the generated adversarial examples have good transferability on the SSD Inception v2 and SSD MobileNet v2 model. For instance, under indoor conditions, the success rates of adversarial examples on the SSD Inception v2 and SSD MobileNet v2 model are 64.44% and 73.33%, respectively. These results are even higher than the success rate on the white-box model. Second, due to the different illumination conditions indoors and outdoors, the transferability of the adversarial examples on the YOLO v2 and YOLO v3 models are different. Under outdoor conditions, the success rates of adversarial examples on the YOLO v2 and YOLO v3 models are 46.67% and 53.33%, which are close to the success rate on the white-box model. Under indoor conditions, the adversarial examples can hardly fool the YOLO v2 and YOLO v3 models. This is because the small perturbations in the adversarial examples cannot be detected by the YOLO v2 and YOLO v3 models in the dark light. Third, for the Faster R-CNN ResNet-50 and Faster R-CNN ResNet-101 models, the success rates of adversarial examples are low both indoors and outdoors. Although the Faster R-CNN Inception v2, Faster R-CNN ResNet-50, and Faster R-CNN ResNet-101 models have the same detection structure, they use different feature extractors extracting different features from the image, which have a great influence on the transferability of the adversarial examples.

Overall, the adversarial examples generated based on the Faster R-CNN Inception v2 model can be successfully transferred to the SSD Inception v2, SSD MobileNet v2, SSD ResNet-50, YOLO v2, and YOLO v3 models.

Table 4: Success rate of adversarial examples on the white-box model and black-box models. The Faster R-CNN Inception v2 model is used as the white-box model, and the Faster R-CNN ResNet-50, Faster R-CNN ResNet-101, SSD Inception v2, SSD MobileNet v2, SSD ResNet-50, YOLO v2, and YOLO v3 models are used as the black-box models.

Model	Success Rate	Success Rate
Wodei	(Indoors)	(Outdoors)
Faster R-CNN Inception v2	33.33%	55.56%
Faster R-CNN ResNet-50	11.11%	2.22%
Faster R-CNN ResNet-101	15.56%	0%
SSD Inception v2	64.44%	48.89%
SSD MobileNet v2	73.33%	28.89%
SSD ResNet-50	22.22%	28.89%
YOLO v2	2.22%	46.67%
YOLO v3	0%	53.33%

6. Conclusion

This paper proposes a robust and natural physical adversarial example attack method for object detectors. We perform a range of image transformations to simulate different physical conditions during the iterative optimization process, to guarantee the robustness of the generated adversarial example. Meantime, for visual naturalness, this paper proposes two novel techniques, the adaptive mask and the real-world perturbation score (RPS), to constrain the added adversarial perturbations. Experimental results in various physical conditions show that, our generated adversarial example can achieve a high attack success rate with natural perturbations. Compared with these existing adversarial example generation methods, the proposed method obtains a good balance between the robustness and the naturalness of the generated adversarial example. In addition, our generated adversarial example is demonstrated to be transferable, which can perform the black-box physical attacks against other deep learning based models. This paper reveals a serious threat, i.e., practical physical adversarial example attack, and further proves the possibility of constructing an adversarial example which is both robust and natural in real-world conditions. Such physical adversarial example attacks will be more difficult to be observed, which highlight the urgency to develop the reliable defense techniques.

References

- Krizhevsky A, Sutskever I, Hinton GE. ImageNet classification with deep convolutional neural networks. In: Proceedings of the Advances in Neural Information Processing Systems. 2012, pp. 1097-1105.
- [2] He K, Zhang X, Ren S, Sun J. Deep residual learning for image recognition. In: Proceedings of the IEEE Conference on Computer Vision and Pattern Recognition (CVPR). 2016, pp. 770-778.
- [3] Greff K, Srivastava RK, Koutník J, Steunebrink BR, Schmidhuber J. LSTM: A search space odyssey. IEEE Transactions on Neural Networks and Learning Systems 2017;28(10):2222-2232.
- [4] Hinton G, Deng L, Yu D, Dahl G, Mohamed AR, Jaitly N, et al. Deep neural networks for acoustic modeling in speech recognition: The shared views of four research groups. IEEE Signal Processing Magazine 2012;29(6):82-97.
- [5] Collobert R, Weston J. A unified architecture for natural language processing: Deep neural networks with multitask learning. In: Proceedings

- of the 25th International Conference on Machine Learning (ICML). 2008, pp. 160-167.
- [6] Kumar A, Irsoy O, Ondruska P, Iyyer M, Bradbury J, Gulrajani I, et al. Ask me anything: Dynamic memory networks for natural language processing. In: Proceedings of the 33th International Conference on Machine Learning (ICML). 2016, pp. 1378-1387.
- [7] Bojarski M, Testa DD, Dworakowski D, Firner B, Flepp B, Goyal P, et al. End to end learning for self-driving cars. arXiv:1604.07316, 2016.
- [8] Chen C, Seff A, Kornhauser A, Xiao J. Deepdriving: Learning affordance for direct perception in autonomous driving. In: Proceedings of the IEEE International Conference on Computer Vision (ICCV). 2015, pp. 2722-2730.
- [9] Faust O, Hagiwara Y, Hong TJ, Lih OS, Acharya UR. Deep learning for healthcare applications based on physiological signals: A review. Computer Methods and Programs in Biomedicine 2018;161:1-13.
- [10] Ravì D, Wong C, Deligianni F, Berthelot M, Andreu-Perez J, Lo B, et al. Deep learning for health informatics. IEEE Journal of Biomedical and Health Informatics 2017;21(1):4-21.
- [11] Szegedy C, Zaremba W, Sutskever I, Bruna J, Erhan D, Goodfellow I, et al. Intriguing properties of neural networks. In: Proceedings of the 2nd International Conference on Learning Representations (ICLR). 2014, pp. 1-10.
- [12] Goodfellow IJ, Shlens J, Szegedy C. Explaining and harnessing adversarial examples. In: Proceedings of the 3rd International Conference on Learning Representations (ICLR). 2015, pp. 1-11.
- [13] Kurakin A, Goodfellow I, Bengio S. Adversarial examples in the physical world. In: Proceedings of the 5th International Conference on Learning Representations (ICLR). 2017, pp. 1-14.
- [14] Carlini N, Wagner D. Towards evaluating the robustness of neural networks. In: Proceedings of the IEEE Symposium on Security and Privacy (S&P). 2017, pp. 39-57.
- [15] Papernot N, McDaniel P, Goodfellow I. Transferability in machine learning: From phenomena to black-box attacks using adversarial samples. arXiv:1604.07316, 2016.
- [16] Zhang J, Li C. Adversarial examples: Opportunities and challenges. IEEE Transactions on Neural Networks and Learning Systems 2020;31(7):2578-2593.
- [17] Yuan X, He P, Zhu Q, Li X. Adversarial examples: Attacks and defenses for deep learning. IEEE Transactions on Neural Networks and Learning Systems 2019;30(9):2805-2824.
- [18] Dong Y, Liao F, Pang T, Su H, Hu X, Li J, et al. Boosting adversarial attacks with momentum. In: Proceedings of the IEEE Conference on Computer Vision and Pattern Recognition (CVPR). 2018, pp. 9185-9193.
- [19] Athalye A, Engstrom L, Ilyas A, Kwok K. Synthesizing robust adversarial examples. In: Proceedings of the 35th International Conference on Machine Learning (ICML). 2018, pp. 284-293.
- [20] Eykholt K, Evtimov I, Fernandes E, Li B, Rahmati A, Xiao C, et al. Robust physical-world attacks on deep learning visual classification. In: Proceedings of the IEEE Conference on Computer Vision and Pattern Recognition (CVPR). 2018, pp. 1625-1634.
- [21] Jan ST, Messou J, Lin YC, Huang JB, Wang G. Connecting the digital and physical world: Improving the robustness of adversarial attacks. In: Proceedings of the 33th AAAI Conference on Artificial Intelligence (AAAI). 2019, pp. 962-969.
- [22] Lu J, Sibai H, Fabry E. Adversarial examples that fool detectors. arXiv:1712.02494, 2017.
- [23] Chen S, Cornelius C, Martin J, Chau DHP. ShapeShifter: Robust physical adversarial attack on faster R-CNN object detector. In: Proceedings of the Machine Learning and Knowledge Discovery in Databases. 2018, pp. 52-68
- [24] Song D, Eykholt K, Evtimov I, Fernandes E, Li B, Rahmati A, et al. Physical adversarial examples for object detectors. In: Proceedings of the 12th USENIX Workshop on Offensive Technologies (WOOT). 2018, pp. 1-10.
- [25] Zhao Y, Zhu H, Liang R, Shen Q, Zhang S, Chen K. Seeing isn't believing: Towards more robust adversarial attack against real world object detectors. In: Proceedings of the ACM SIGSAC Conference on Computer and Communications Security (CCS). 2019, pp. 1989-2004.
- [26] Ren S, He K, Girshick R, Sun J. Faster R-CNN: Towards real-time object detection with region proposal networks. IEEE Transactions on Pattern Analysis and Machine Intelligence 2017;39(6):1137-1149.

- [27] Liu W, Anguelov D, Erhan D, Szegedy C, Reed S, Fu CY, et al. SSD: Single shot multibox detector. In: Proceedings of the 14th European Conference on Computer Vision. 2016, pp. 21-37.
- [28] Redmon J, Farhadi A. YOLO9000: Better, faster, stronger. In: Proceedings of the IEEE Conference on Computer Vision and Pattern Recognition (CVPR). 2017, pp. 6517-6525.
- [29] Redmon J, Farhadi A. YOLOv3: An incremental improvement. arXiv:1604.07316, 2018.
- [30] Girshick R, Donahue J, Darrell T, Malik J. Rich feature hierarchies for accurate object detection and semantic segmentation. In: Proceedings of the IEEE Conference on Computer Vision and Pattern Recognition (CVPR). 2014, pp. 580-587.
- [31] Girshick R. Fast R-CNN. In: Proceedings of the IEEE International Conference on Computer Vision (ICCV). 2015, pp. 1440-1448.
- [32] Redmon J, Divvala S, Girshick R, Farhadi A. You only look once: Unified, real-time object detection. In: Proceedings of the IEEE Conference on Computer Vision and Pattern Recognition (CVPR). 2016, pp. 779-788.
- [33] Lu J, Sibai H, Fabry E, Forsyth D. No need to worry about adversarial examples in object detection in autonomous vehicles. arXiv:1707.03501, 2017.
- [34] Huang L, Gao C, Zhou Y, Zou C, Xie C, Yuille A, et al. UPC: Learning universal physical camouflage attacks on object detectors. arXiv:1909.04326, 2019.
- [35] Huang Y, Kong AW, Lam K. Adversarial signboard against object detector. In: Proceedings of the 30th British Machine Vision Conference (BMVC). 2019, pp. 231-241.
- [36] Lee M, Kolter JZ. On physical adversarial patches for object detection. arXiv:1906.11897, 2019.
- [37] Li J, Schmidt FR, Kolter JZ. Adversarial camera stickers: A physical camera-based attack on deep learning systems. In: Proceedings of the 36th International Conference on Machine Learning (ICML). 2019, pp. 3896-3904.
- [38] Wikipedia . CMYK color model. 2019. URL: https://en.wikipedia.org/wiki/CMYK_color_model.
- [39] Lin T, Maire M, Belongie SJ, Hays J, Perona P, Ramanan D, et al. Microsoft COCO: Common objects in context. In: Proceedings of the 13th European Conference on Computer Vision. 2014, pp. 740-755.
- [40] Sharif M, Bhagavatula S, Bauer L, Reiter MK. Accessorize to a crime: Real and stealthy attacks on state-of-the-art face recognition. In: Proceedings of the 2016 ACM SIGSAC Conference on Computer and Communications Security. 2016, pp. 1528-1540.
- [41] Huang J, Rathod V, Sun C, Zhu M, Korattikara A, Fathi A, et al. Speed/accuracy trade-offs for modern convolutional object detectors. In: Proceedings of the IEEE Conference on Computer Vision and Pattern Recognition (CVPR). 2017, pp. 3296-3297.
- [42] Pkulzc VR, Wu N. Tensorflow detection model zoo. 2019. URL: https://github.com/tensorflow/models/blob/master/ research/object_detection/g3doc/detection_model_zoo.md.
- [43] Carlini N, Wagner D. Adversarial examples are not easily detected: By-passing ten detection methods. In: Proceedings of the 10th ACM Workshop on Artificial Intelligence and Security. 2017, pp. 3-14.
- [44] Redmon J, Farhadi A. YOLO: Real-time object detection. 2018. URL: https://pjreddie.com/darknet/yolo.